Single beam laser induced fluorescence technique for plasma transport measurements

D. A. Edrich, R. McWilliams, and N. S. Wolf

Citation: Review of Scientific Instruments **67**, 2812 (1996); doi: 10.1063/1.1147111
View online: http://dx.doi.org/10.1063/1.1147111
View Table of Contents: http://scitation.aip.org/content/aip/journal/rsi/67/8?ver=pdfcov
Published by the AIP Publishing

Single beam laser induced fluorescence technique for plasma transport measurements

D. A. Edrich and R. McWilliams
Department of Physics and Astronomy, University of California, Irvine, California 92717

N. S. Wolf
Department of Physics and Astronomy, Dickinson College, Carlisle, Pennsylvania 17013

(Received 27 April 1995; accepted for publication 22 April 1996)

A technique for measuring ion transport using laser-induced fluorescence has been developed and tested in an argon plasma. It uses only one broadband beam thus being simpler than some previous techniques because no detection beam is required. First, a 5 μs laser pulse centered on 611 nm stimulates a transition from the metastable state in Ar(II) $3d\ ^2G_{9/2}$ to $4p\ ^2F^0_{7/2}$. A $4p\ ^2F^0_{7/2}$ to $4s^2D_{5/2}$transition rapidly results with emission at 461 nm. Upon cessation of the laser pulse, the 461 nm light in the detection volume does not return to its background level immediately because the $3d\ ^2G_{9/2}$ level is partially depleted. The time history of the 461 nm signal in returning to steady-state background intensity provides a means of determining ion transport because the recovery signal is due to processes including ion excitation, diffusion, convection, and thermal motion. Measurements of the ion velocity distribution yield the contributions of thermal and convective effects to ion transport. By varying the laser beam diameter and the detection volume the plasma ion spatial diffusion coefficient *D*, and the time, τ_p it takes for processes other than transport to bring the 461 nm emission back to the steady-state background level are determined. For example, in one set of plasma conditions $D=0.58\pm0.16$ m^2/s and $\tau_p=59\pm7$ μs were found. [S0034-6748(96)00108-6]

I. INTRODUCTION

Laser induced fluorescence (LIF) plasma diagnostics have been developed and fielded for a variety of purposes. LIF is a nonperturbing, *in situ* diagnostic capable of measuring ion velocity distributions (including convection),[1–6] direct ion transport,[7] spatial diffusion,[8–11] velocity space diffusion and stochastic heating,[12–16] and phase space densities.[17,18]

The technique described in this article relies upon a reduction of detected intensity due to a laser ion tagging process. A technique previously described by Stern, Hill, and Rynn[7] includes a method which relies upon signal reduction as well. In Ref. 7 ions are used which have two long-lived states, O and B (e.g., ground and metastable), mutually accessible through an excited state, A. Reference 7 describes two methods by which tagging and subsequent detection of tagged ions can be achieved. In the first method, which the authors dub ''dark'' tagging, a pump laser depletes the population in O and raises the population in B via excitation of the OA transition. When a second laser, tuned to the OA transition, later shines upon ions the fluorescence intensity reduces compared to the intensity induced by the second beam when the pump laser is off (hence the dark label). This reduction in the second LIF intensity allows a measure of transport, in time and space, of those ions which were tagged by the pump laser. The second method, dubbed ''bright'' tagging uses the same pump laser transition excitation but calls for the second laser to be tuned to the BA transition. The B state has its population increased by the action of the pump laser so that the second LIF intensity is increased compared to the intensity induced by the second beam when the pump is off (hence the bright label). Again, ion transport information may be gained by this interrogation process.

This article describes a method of ion tagging and detection which utilizes only one laser beam. There is some conceptual overlap with the first technique of Ref. 7. In related work, Refs. 15 and 16 determine velocity space diffusion coefficients by following the time evolution of a fluorescence signal while the laser, run in single mode, is on. Briefly, the technique described below uses a single laser beam in combination with the background emission from the plasma to determine the spatial diffusion coefficient of the plasma ions. The steady-state background emission intensity of a line from the plasma ions is measured. Then a broadband laser pulse is used to deplete locally a state contributing to the detected intensity. Upon termination of the laser pulse the background intensity is found to be reduced compared to the steady-state level. In time the background line intensity returns to the steady-state value in the detection volume due to tagged ion diffusion, convection, thermal effects, and atomic physics processes. By using various optics combinations the ion diffusion coefficient *D* and the time τ_p it takes for processes other than transport to bring the 461 nm emission back to the steady-state background level can be determined if the ion distribution function is known. The ion distribution function can be measured using the laser system in single-mode operation.

II. LIF SCHEME

LIF as used here is a two-step process. First a laser excites a valence electron from a populated metastable state to a short-lived higher state. A fraction of these excited electrons make the transition to a third state, emitting a photon in the process. These photons have a different frequency than

 0034-6748/96/67(8)/2812/6/$10.00

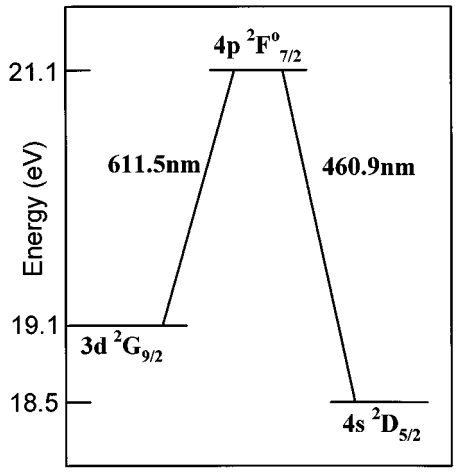

FIG. 1. Electrons in the $3d\ ^2G_{9/2}$ metastable state were excited to the $4p\ ^2F^0_{7/2}$ state with a laser. Photons from those electrons that decay to the $4s\ ^2D_{5/2}$ state were collected with a PMT.

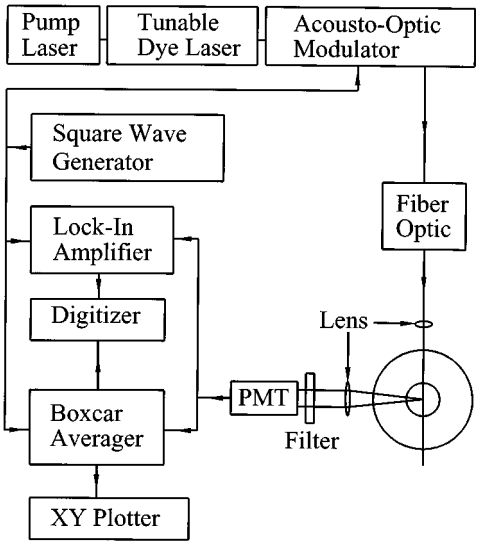

FIG. 2. Schematic of LIF diagnostic equipment.

the source laser. Their intensity is proportional to the density of ions with metastable state electrons in the excitation laser beam region.

For LIF in argon we used the scheme displayed in Fig. 1. Table I provides relevant data about the states and transitions of this LIF scheme. The $3d\ ^2G_{9/2}$ state is a metastable state which can be excited to the $4p\ ^2F^0_{7/2}$ state by a 611 nm photon. The $4p\ ^2F^0_{7/2}$ state has a lifetime of 7.4 ns and can decay to the $4s\ ^2D_{5/2}$ state by emitting a photon of 461 nm[19] which can be collected with a photomultiplier tube (PMT). Because the $4s\ ^2D_{5/2}$ state has a dipole transition to the ground state of Ar(II), the plasma does not absorb the 461 nm photons. Since the $3d\ ^2G_{9/2}$ state is elevated above the $4s\ ^2D_{5/2}$ state, photons of higher energy are emitted compared to those absorbed from the laser. Two advantages to this scheme are that 611 nm is attainable with rhodamine 6G dye, a long lasting and stable laser dye, and 461 nm is in a region of high efficiency for PMTs.

An argon plasma was created by ionizing a neutral argon gas ($P=10^{-4}$ Torr) with steady-state electron beams. Metastable state creation and depletion thus were ongoing processes, creating a background source of light at many wavelengths, including 461 nm. This background was proportional to the ion density and swamped the LIF signal.

TABLE I. Data on LIF scheme (Refs. 19, 30–32).

Parameter	Absorbed	Emitted
Wavelength (nm)	611.492 34	460.95 673
Absolute transition probability (MHz)	21.2 ± 0.5	75.9 ± 12
Natural linewidth (MHz)	21.6	27.4
Zeeman lines	24	18

Electron state	$3d\ ^2G_{9/2}$	$4p\ ^2F^0_{7/2}$	$4s\ ^2D_{5/2}$
Gyromagnetic ratio g	10/9	8/7	6/5
Nondegenerate states	10	8	6
Energy level (cm^{-1})	154 181.51	170 531.29	148 842.45
Lifetime (ns)	metastable	7.359	27.6

The LIF signal was recovered by modulating the input laser beam and detecting the signal with either a lock-in amplifier or a gated integrator.

III. INPUT OPTICS

The input apparatus consisted of three parts: laser, fiber optics, and focusing head. A Lexel Model 95 argon ion laser capable of 4.5 W pumped a Coherent CR 599-21 scanning single frequency dye laser to provide stable and remotely controllable laser light. Rhodamine 6G dye was used to achieve the 611 nm wavelength, providing up to 900 mW of broadband and 200 mW of single-mode output power with a dye lifetime of over a 1000 W/h. Typical output levels were 750 mW broadband and 70 mW single-mode. The dye laser output was modulated at 100 kHz with an Isomet Model 1206C acousto-optic modulator for single-mode measurements yielding the ion velocity distribution function. For broadband tagging the acousto-optic modulator was used to make a 5 μs laser beam pulse repeated no more than every 50 μs. Figure 2 is a schematic of the equipment used for this LIF diagnostic.

After modulation, a fiber-optic cable carried the laser light to the vessel. The modulated laser light was focused into a 100-μm-diam 75-m-long silica fiber. At the other end of the fiber a collimator refocused the light into a parallel beam directed through the plasma.

The beam radius was varied by changing focusing heads on the collimator. The refocused laser power profile was measured and can be approximated by a Gaussian. The root mean square (rms) values of the radius r_{laser} were measured as 1.49, 1.06, and 0.46 mm for no focusing head, 1 m focusing head, and 20 cm focusing head, respectively, at the center of the plasma target volume 15 cm from the focusing head.

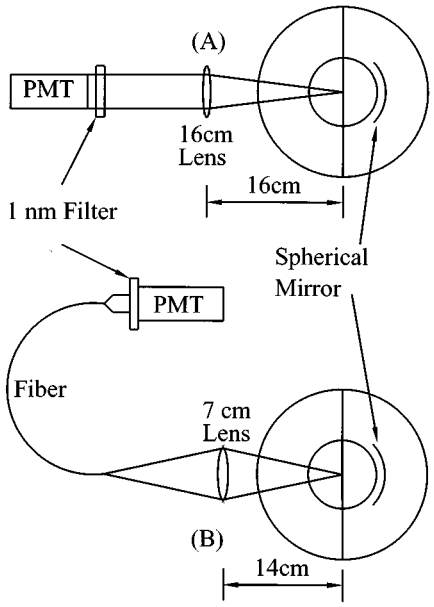

FIG. 3. System A places light source at focal length of lens. System B places light source at twice the focal length from lens.

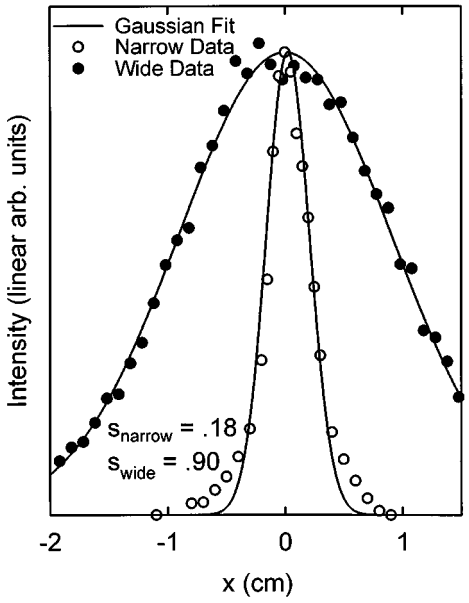

FIG. 4. LIF signal vs radius from target point for System A with 16 cm focal width lens (dots), and System B with a 7 cm focal width and fiber optic (open circles).

IV. COLLECTION OPTICS

Two arrangements of collection optics were used. System A was designed to maximize collected light and System B was designed to optimize spatial resolution. Both arrangements are shown in Fig. 3. System A used a 16 cm focal length convex lens. The lens was placed outside the vacuum vessel 16 cm from the target plasma and just beyond a variable aperture. With the target at the focal point, light from the target was refracted parallel to the axis of the lens. After the lens, a light-tight tube carried the light 33 cm out of the confining magnetic field. This light was passed through a 1 nm filter centered at 461.3 nm, with a 3° acceptance angle, so light originating from a small volume centered on the target passed through the filter. Behind the filter, a 1.5-in.-diam PMT collected light that passed through the filter. The radius of the collection volume was measured by scanning a cw 0.46 mm rms radius 611 nm wavelength broadband laser beam across the target plasma volume and recording the LIF signal. By varying the aperture the profiles were measured to be Gaussian normal to the lens axis with rms radii, r_{optics}, from 3.58 to 9.00 mm normal to the lens axis. An example of the measured profile with the 9 mm width is shown in Fig. 4. Measurements of the detection volume depth (along the lens axis) were made by moving the optics towards and away from the laser beam position while holding the laser beam position constant. The rms radius of depth was found to exceed 5 cm.

System B used a 7 cm focal length lens. The lens was placed outside the vacuum vessel 14 cm from the target. Light from the target area was focused 14 cm behind the lens onto a 1 mm diam fiber optic cable. At the other end of the fiber a collimator focused the light into a parallel beam. This beam was passed through the 1 nm filter and onto the PMT. As shown in Fig. 3, a scan of this optics arrangement had a rms radius of 1.8 mm normal to the lens axis.

Although System B gave higher spatial resolution, System A has advantages as well. The larger collection volume of System A gave more spatial averaging over fluctuations in the plasma and when combined with larger diameter laser beams gave a larger LIF signal. Losses due to coupling into the fiber optic in System B also lowered the collected light. Unless optimum spatial resolution was required, System A was used for data collection.

Both systems used a spherical concave radius mirror inside the vacuum vessel. This mirror was 3.5 cm in diameter and had a 5 cm radius of curvature. Its symmetry axis was aligned with the axis of the collection optics lens and its center of curvature was collocated at the source of light or target point. With the target located at the plasma center the mirror was outside the plasma column. It reflected back toward the target the solid angle of light that intersected it, thus increasing the light collected by the collection lens.

V. BROADBAND AND SINGLE-MODE MEASUREMENTS

A broadband laser was used to excite Doppler broadened ions from the metastable state. The instantaneous light from the Coherent 599 laser (without the etalon cavity) has a bandwidth that does not cover the entire absorption line. However, the laser center frequency was continuously and rapidly changing with each mode hop the laser cavity made. In time, this center frequency covers all frequencies in a large band about a peak value. If a time average of the LIF signal was made with the laser peak centered on the 611 nm absorption line, then all $3d\ ^2G_{9/2}-4p\ ^2F^0_{7/2}$ transitions are excited regardless of the Doppler shift.

Using the dye laser in single-mode operation, velocity distributions were measured as described by Hill, Fornaca, and Wickham.[5] An absolute measure of the convective velocity was obtained by comparing the vertical ion velocity

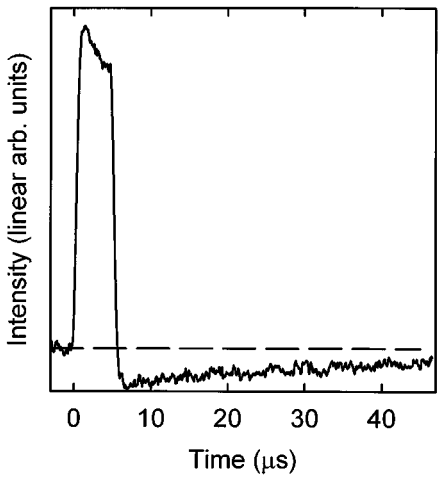

FIG. 5. 461 nm line intensity vs time. During the laser pulse the metastable state was depleted. After the pulse was terminated, the line intensity reduced below background. The dashed line gives the unperturbed background light level.

distributions taken with the laser beam pointing vertically up and then vertically down through the plasma. For the axial and radial measures, the most recent vertical measurement provided a zero velocity reference laser frequency. The largest drift was in the vertical direction.

VI. RECOVERY TAGGING

A signal increase was observed when the laser pulse was on. After the laser pulse was terminated, the 461 nm line intensity dropped below background and then recovered to its initial value. The characterization of the return (including half-life) of this signal drop, or recovery, from below background to background value provides a means of determining ion transport because the signal recovery is due to several processes, including ion excitation, and both ion diffusion and ion thermal motion into the detection region.

Figure 5 gives a sample LIF signal versus time for a laser pulse. The background intensity level can be observed for times less than $t=0$ in the figure. At $t=0$ the laser pulse is turned on resulting in increased fluorescence. This increased fluorescence intensity reduces somewhat while the laser is on due to depletion of the available metastable ion population in the illuminated volume.[15,16,20] Following termination of the laser signal at $t=5$ μs the detected intensity falls below the background level. The intensity is seen to return to the background level over a period of tens of microseconds. Electrons in the $3d\ ^2G_{9/2}$ state are available to contribute to the 461 nm intensity via plasma and electron beam excitation processes. When this metastable state is depleted the 461 nm intensity is reduced until transport and atomic processes restore the metastable population in the detection volume to its original level. All other sources of background 461 nm light are unperturbed in this LIF process. This below-background intensity recovery signal is thus an indicator of the presence of metastable-depleted ions.

Throughout the argon plasma metastable ions were continuously created by the electron beam plasma formation process and destroyed through atomic processes of collisions, recombination, and charge exchange. Metastable ion populations perturbed by LIF would return, due to atomic processes, to the background steady-state population with an exponential time constant for each atomic process. When several processes contribute to the return to steady-state metastable population the reciprocal of the exponential time constant is the sum of the reciprocal individual process time constants. This decay time, τ_p, of the perturbed ions fixes an upper limit on temporal usefulness of metastable perturbations for transport measurements. If ions remain tagged long enough to diffuse or convect noticeably out of the detection volume then transport coefficients may be determined. Conversely, if the time for atomic processes to refill the depleted metastable state ion population is less than the time for ions to diffuse or convect noticeably out of the detection volume then this tagging scheme will not yield transport coefficients.

VII. ION TRANSPORT

Chandrasekhar derived the probability distribution W for a particle's current position, $\mathbf{r}$, as a function of initial position, $\mathbf{r}_0$. initial velocity, $\mathbf{v}_0$, and time, t, from the Langevin equation,[21]

$$W(\mathbf{r},t;\mathbf{r}_0,\mathbf{v}_0)=\left\{\frac{m\nu^2}{2\pi kT[2\nu t-3+4e^{-\nu t}-e^{-2\nu t}]}\right\}^{3/2}\times\exp\left(-\left\{\frac{m\nu^2|\mathbf{r}-\mathbf{r}_0-\mathbf{v}_0(1-e^{-\nu t})/\nu|^2}{2kT[2\nu t-3+4e^{-\nu t}-e^{-2\nu t}]}\right\}\right), \tag{1}$$

where ν is the frequency of collisions and m is the ion mass. Since we are working with a subset of ions that are in thermal equilibrium at temperature T, the velocity distribution is in general Maxwellian. We can integrate the product of Eq. (1) and a Maxwellian velocity distribution over all possible initial velocities to get the probability distribution averaged over initial velocity. The result

$$W(\mathbf{r},t;\mathbf{r}_0)=\left\{\frac{m\nu^2}{4\pi kT[\nu t-1+e^{-\nu t}]}\right\}^{3/2}\times\exp-\left\{\frac{m\nu^2|\mathbf{r}-\mathbf{r}_0|^2}{4kT[\nu t-1+e^{-\nu t}]}\right\} \tag{2}$$

has a mean squared value for the radius of

$$\langle|\mathbf{r}-\mathbf{r}_0|^2\rangle=6kT[\nu t-1+e^{-\nu t}]/m\nu^2. \tag{3}$$

For values of $\nu t\gg 1$, this simplifies to $\langle|\mathbf{r}-\mathbf{r}_0|^2\rangle = 6kTt/m\nu=6Dt$ with $D=kT/m\nu$. This model of D applies for the case of $\nu^2\gg\omega_{ci}^2$ where ω_{ci} is the ion cyclotron frequency. For the experimental conditions ($B=1$ kG, argon ions) $\omega_{ci}=2.4\times10^5$ s^{-1} and ν was found to be above 1 MHz. In the short time case, $\nu t\ll 1$, the mean squared radius simplifies to $3kTt^2/m$ and is due to free streaming or unimpeded thermal ion motion.

In the experiment a vertical column of metastable ions is tagged with a pulse of laser light. Let the z axis be along the laser beam in the vertical direction. Let the y axis be along the collection optics axis (normal to the z axis) and the x axis be normal to both the y and z axes. The collection optics are focused to the center of the plasma where the plasma prop-

erties are approximately uniform over the plasma observed by the collection optics. By tagging a vertical column the vertical dimension thus is removed from the analysis since the vertical translational invariance implies that, on average, for every tagged ion which moves vertically out of the collection optics volume there will be another which enters from the opposite side above or below. Such a distribution of deexcited metastables will drift with measurable convective velocities v_{xc} and v_{yc} normal to the laser beam. A Gaussian tagged ion distribution in two dimensions, initially centered at the origin, takes the form

$$f(x-v_{xc}t,y-v_{yc}t,t)=\frac{1}{2\pi\langle(\delta r)^2\rangle}\times\exp\left\{-\frac{(x^2+y^2)}{2\langle(\delta r)^2\rangle}-\frac{t}{\tau_p}\right\}, \quad (4)$$

with an exponential decay that accounts for tagged ions lost due to effects other than transport and where $\langle(\delta r)^2\rangle$ is the mean squared radius in the *xy* plane of the tagged ions. The drifts v_{xc} and v_{yc} perpendicular to the vertical were measured and found to be ignorable for the time scale of the measurements. The depth of field of the collection optics further simplifies the analysis by one dimension since any motion of the ions in the *y* direction will retain the ions within the observed volume during the experiment time. Hence, only ion transport in the *x* direction will lead to changes in detected intensity.

For times after the termination of the laser pulse the reduction of signal below the steady-state background intensity collected by the PMT is calculated by combining the tagged ion distribution (a Gaussian function of *x* and *y*) and the spatial sensitivity of the collection optics (a Gaussian function of *x* and *z*). Their product (for a distribution created at $t=0$), when integrated over all space, gives

$$I_{\rm loss}=A\ \exp\left(\frac{-t}{\tau_p}\right)\ \Big/\ \sqrt{r_{\rm optics}^2+\langle(\delta x)^2\rangle} \quad (5)$$

for the amount of reduction of the detected intensity, $I_{\rm loss}$, below the steady-state background intensity, and where $\langle(\delta x)^2\rangle$ is the mean squared spread of the tagged ions in the *x*-direction. Thus, $I_{\rm loss}$ is the difference between steady-state background intensity and the observed intensity in the signal recovery period. *A* is a normalization factor and $r_{\rm optics}$ is the rms radius of the optics sensitivity normal to the collection optics axis.

The laser beam had a measured Gaussian power profile, therefore the initial distribution of metastable depleted ions should have this same shape (for all measurements the total laser induced metastable depletion was less than 20%, and broadband (>30 GHz) laser power was less than 100 mW into more than 1 $\rm mm^2$ at the plasma, well below saturation[20,22–24]),

$$\langle(\delta x)^2\rangle_{t=0}=r_{\rm laser}^2. \quad (6)$$

The laser was applied for 5 μs. Two microseconds after laser pulse termination were required for the integrating electronics to remove the laser-on signal from the recovery signal. A small number of tagged ions were created throughout the 5 μs laser pulse. At each instant in time during the pulse a tagged ion population was created which then experienced transport and metastable refilling as time continued after that instant. At any time *t* after the instant of tagged ion creation that particular set of tagged ions would spread in space according to

$$\langle(\delta x)^2\rangle=r_{\rm laser}^2+2kT[\nu t-1+e^{-\nu t}]/m\nu^2. \quad (7)$$

The total ion spatial distribution after signal stabilization, 2 μs after the end of the laser pulse, is a sum of the tagged spreading ion distributions, created at each instant throughout the 5 μs pulse, experiencing transport and refilling from time of creation to time of observation. In the above equations time *t* refers to the time between tagged ion creation and observation. Since the creation period is 5 μs long, tagged ions created during the laser pulse would have different *t*'s at the moment when the observation was made. Rather than have time defined multiply, we choose the following convention for time notation: for data analysis and computational modeling *t* will represent the time from signal stabilization to moment of observation. The time duration from tagged ion creation to moment of observation will now be represented as $t+t_c$.

The number of tagged ions created at any given time is proportional to the LIF detected intensity $I_{\rm laser}$, at 461 nm during the laser pulse. The contribution to the detected intensity reduction at time *t* after signal stabilization from the tagged ion population created at time t_c prior to stabilization is

$$I_{\rm loss}(t,t_c)\propto\{r_{\rm optics}^2+r_{\rm laser}^2+2kT\times[\nu(t+t_c)-1+e^{-\nu(t+t_c)}]/m\nu^2\}^{-1/2}\times e^{-(t+t_c)/\tau_p}. \quad (8)$$

The observed reduction from background intensity is thus

$$I_{\rm loss}(t)=A\int_{2\mu\rm s}^{7\mu\rm s}I_{\rm loss}(t,t_c)dt_c, \quad (9)$$

where *A* is chosen so that $I_{\rm loss}(0)=1$.

VIII. EXPERIMENTAL APPLICATION AND DISCUSSION

A gated integrator recorded the 461 nm fluorescence signal as a function of time (see Fig. 2). Figure 6 shows a measurement of $I_{\rm loss}(t)$ beginning 7 μs after the beginning of the laser pulse until about 48 μs. The trend for the signal to return to background level (shown as 0 in the figure) is clear. A curve fitter using the Marquardt–Levenberg least-squares algorithm[25] was used to fit the experimental data to determine the best fit values of *D* and τ_p for the Eq. (9) fit for $I_{\rm loss}(t)$ and utilizing $D=kT/m\nu$. The best values fit were $D=0.58\pm0.16$ $\rm m^2/s$ and $\tau_p=59\pm7$ μs. The prediction of $I_{\rm loss}(t)$ using these values is shown as the dashed curve in the figure. One sees agreement, within the experimental noise level and over the entire observation time, between the theoretical curve using these values and the experimental values. The value of *D* is similar to diffusion values obtained from laboratory plasmas where turbulence is thought to dominate transport over classical collisional processes.[10,26] A value of

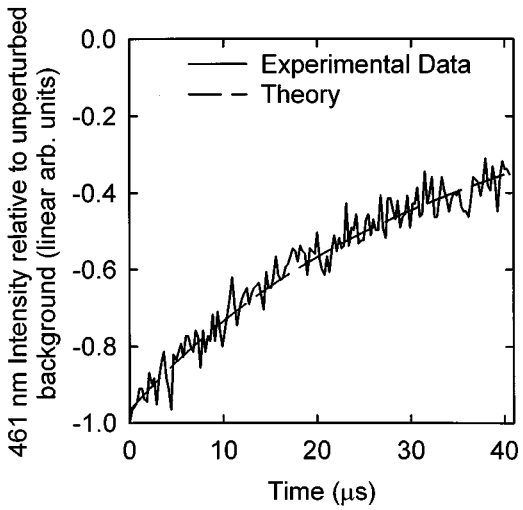

FIG. 6. Comparison of observed 461 nm line intensity to value predicted by theory [Eq. (9)] using $D=0.58\pm0.16$ m^2/s and $\tau_p=59\pm7$ μs.

$D=0.58\pm0.16$ m^2/s implies a collision frequency of 1.6 MHz for the 0.4 eV temperature ions. The ion–ion Coulomb collision frequency is about 5 kHz for the plasma densities of about 10^{16} m^{-3} studied here. Elastic collisions of ions with neutrals[27] and charge exchange[28] were estimated to be less frequent. Hence, classical collisional processes do not play a dominant role in the diffusion measured here. McChesney[29] made preliminary measurements in an argon plasma with different plasma parameters and generation techniques, by use of two lasers, and of the tagged signal versus time for the Encore Tokamak. The signals he observed had e-folding times of about 3 μs and were not utilized to estimate diffusion coefficients.

Another method for finding D and τ_p was to vary the laser beam and collection optics sizes, while holding plasma parameters constant, and characterizing $I_{\rm loss}(t)$ by measuring the time $\tau_{1/2,\rm experiment}$, required for $I_{\rm loss}(t)$ to go to $I_{\rm loss}(0)/2$, i.e., to decay by half. A Marquardt–Levenberg least squares algorithm[25] was used to determine the best fit values of D and τ_p for the variety of optics sizes. A comparison of the prediction from Eq. (9) for the decay-by-half time, $\tau_{1/2,\rm theory}$ using the fitted D and τ_p along with the measured $r_{\rm optics}$ and $r_{\rm laser}$, versus the measured $\tau_{1/2,\rm experiment}$ is shown in Fig. 7, with the solid line representing unity correlation. For a linear fit the correlation coefficient is $r^2=0.93$. We note that the comparison technique used for Fig. 6 shows closer agreement between theory and experiment. This first technique utilizes the full set of data points rather than just the decay-by-half time and hence has a far larger data set with which to work.

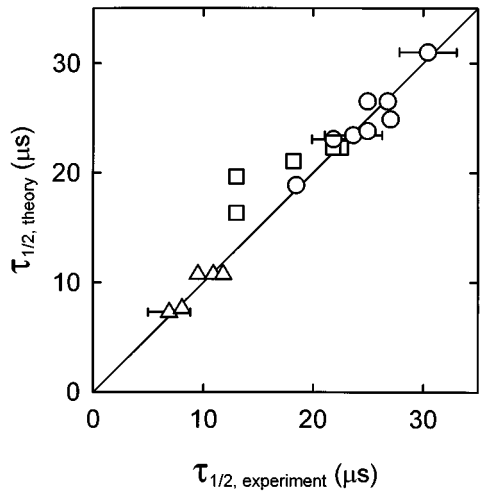

FIG. 7. Measured half-life of $I_{\rm loss}$ vs the calculated value. The parameters τ_p and D were chosen to optimize the correlation between theory and experiment.

ACKNOWLEDGMENTS

The authors acknowledge useful discussions with P. Bellan, A. Bailey, D. Sheehan, and R. Stern. This work was supported by NSF Grant No. 94-19192.

[1] E. Hinnov, J. G. Hirschberg, F. W. Hofmann, and N. Rynn, Phys. Fluids **6**, 1779 (1963).
[2] F. W. Hofmann, Phys. Fluids **7**, 532 (1964).
[3] D. Dimock, E. Hinnov, and L. C. Johnson, Phys. Fluids **12**, 1730 (1969).
[4] R. A. Stern and J. A. Johnson, Phys. Rev. Lett. **34**, 1548 (1975).
[5] D. N. Hill, S. Fornaca, and M. G. Wickham, Rev. Sci. Instrum. **54**, 309 (1983).
[6] M. J. Goeckner, J. Goree, and T. E. Sheridan, Phys. Fluids B **3**, 2913 (1991).
[7] R. A. Stern, D. N. Hill, and N. Rynn, Phys. Lett. A **93**, 127 (1983).
[8] R. McWilliams, D. H. Hill, N. S. Wolf, and N. Rynn, Phys. Rev. Lett. **50**, 836 (1983).
[9] R. McWilliams and M. K. Okubo, Phys. Fluids **30**, 2849 (1987).
[10] R. McWilliams, M. K. Okubo, and N. S. Wolf, Phys. Fluids B **2**, 523 (1990).
[11] A. Fasoli, F. Skiff, T. N. Good, and P. J. Paris, Phys. Rev. Lett. **68**, 2925 (1992).
[12] J. M. McChesney, P. M. Bellan, and R. A. Stern, Phys. Fluids B **3**, 3363 (1991).
[13] J. Bowles, R. McWilliams, and N. Rynn, Phys. Rev. Lett. **68**, 1144 (1992).
[14] J. Bowles, R. McWilliams, and N. Rynn, Phys. Plasmas **1**, 3814 (1994).
[15] F. Skiff and J. J. Curry, Rev. Sci. Instrum. **66**, 629 (1995).
[16] J. J. Curry, F. Skiff, M. Sarfaty, and T. N. Good, Phys. Rev. Lett. **74**, 1767 (1995).
[17] R. McWilliams and D. Sheehan, Phys. Rev. Lett. **56**, 2485 (1986).
[18] A. Fasoli *et al.*, Phys. Rev. Lett. **63**, 2052 (1989).
[19] G. Garcia and J. Campos, J. Quant. Spectrosc. Radiat. Transfer **34**, 85 (1985).
[20] D. N. Hill, Ph.D. thesis, University of California, Irvine, 1983.
[21] S. Chandrasekhar, Rev. Mod. Phys. **15**, 1 (1943).
[22] R. A. Stern, Phys. Fluids **21**, 1287 (1978).
[23] P. G. Pappas, M. M. Burns, D. D. Hinshelwood, M. S. Field, and D. E. Murnick, Phys. Rev. A **21**, 1955 (1980).
[24] M. J. Goeckner and J. Goree, J. Vac. Sci. Technol. A **7**, 977 (1989).
[25] J. Kuo, E. Fox, D. Mitchell, and T. Tuerke, *Sigma Plot Scientific Graph System: Transforms and Curve Fitting Reference*, 5.0 ed. (Jandel Corporation, 1992).
[26] W. Horton and W. Rowan, Phys. Plasmas **1**, 901 (1994).
[27] W. H. Cramer, J. Chem. Phys. **30**, 641 (1959).
[28] S. C. Brown, *Basic Data of Plasma Physics*, 2nd ed. (MIT Press, Cambridge, 1966).
[29] J. M. McChesney, Ph.D. thesis, California Institute of Technology, 1989.
[30] R. L. Kelly, J. Phys. Chem. Ref. Data **16**, Supp. No. 1 (1987).
[31] G. Norlén, Phys. Scr. **8**, 249 (1973).
[32] B. F. J. Luyken, Physica **60**, 432 (1972).